Journal of Physics and Chemistry of Solids 87 (2015) 271–277

Contents lists available at ScienceDirect

Journal of Physics and Chemistry of Solids

journal homepage: www.elsevier.com/locate/jpcs

Stability of anti-reflection coatings via the self-assembly encapsulation of silica nanoparticles by diazo-resins

Jonathan S. Metzman [a], Jason I. Ridley [b], Moataz B. Khalifa [b], James R. Heflin [b,*]

[a] Department of Materials Science and Engineering, Virginia Tech, Blacksburg, VA 24061, USA
[b] Department of Physics, Virginia Tech, Blacksburg, VA 24061, USA

ARTICLE INFO

Article history:
Received 12 May 2015
Received in revised form
28 August 2015
Accepted 3 September 2015
Available online 8 September 2015

Keywords:
A. Multilayers
A. Nanostructures
A. Polymers
D. Optical properties

ABSTRACT

A modified silica nanoparticle (MSNP) solution was formed by the encapsulation of negatively charged silica nanoparticles by the UV-crosslinkable polycation oligomer diazo-resin (DAR). Appropriate DAR encapsulation concentrations were determined by use of zeta-potential and dynamic light scattering measurements. The MSNPs were used in conjunction with poly(styrene sulfonate) (PSS) to grow homogenous ionic self-assembled multilayer anti-reflection coatings. Stability was induced within the films by the exposure of UV-irradiation that allowed for crosslinking of the DAR and PSS. The films were characterized by UV/vis/IR spectroscopy and field emission scanning electron microscopy. The transmission and reflection levels were $>98.5\%$ and $<0.05\%$, respectively. The refractive indices resided in the 1.25–1.26 range. The solvent stability was tested by sonication of the films in a ternary solvent (H_2O/DMF/$ZnCl_2$ 3:5:2 w/w/w).

1. Introduction

Anti-reflection coatings (ARCs) are commonly used to reduce substrate reflection, while maximizing transmission, in the visible wavelength range of incident light. Along with a decrease in loss of transmitted light, ARCs diminish glare created by high levels of reflected light. ARCs must fulfill two conditions to exhibit zero reflectance due to destructive interference (1) OT$=\lambda/4$ and (2) $n_c = \sqrt{n_1 n_2}$ where OT is the optical thickness of the coating (product of the physical thickness and refractive index), λ is the desired wavelength in nm, n_c is the refractive index of the coating, and n_1 and n_2 refer to the refractive indices of the media on either side of the coating. Condition (1) creates a π-phase shift between light reflected off the underlying substrate and the light reflected off the coating, resulting in destructive interference. Condition (2) ensures that the amplitudes of the reflected electromagnetic waves from the upper and lower ARC coating surfaces are equal. In the commonplace example that the substrate is composed of glass ($n=1.50$) and the surrounding medium is air ($n=1.0$), the refractive index of the coating should be $n_c=1.22$. Condition (1) is far less stringent to accomplish, as modern methods of film growth can precisely control thickness, whereas condition (2) requires control on the composition of the coating, which is not as variable, comparatively. Single-layer ARCs consist of one transparent dielectric material for low reflectance in a narrow range of wavelengths. MgF_2 is typically used for single-layer ARCs on glass due to its low index of refraction at $n=1.38$. At this refractive index value, MgF2 ARCs reduce the reflectance on a glass substrate from approximately 4–1.2% per surface.

A wide range of deposition techniques have been utilized for ARCs including sol–gel synthesis [1,2], nano-imprint lithography [2,3], plasma-enhanced chemical vapor deposition[4], e-beam evaporation[5], spin coating[6], and chemical etching [7]. Although these methods feature a range of pros and cons, the most common drawbacks relate to high cost and complexity in growth (especially for concave or flexible substrates). Layer-by-layer ionic self-assembled multilayers (ISAMs) address these issues due to the versatility of deposition and their relatively inexpensive nature. The formation of ISAM films relies on electrostatic attraction, hydrogen bonding, and secondary forces and occurs through alternating immersion of a charged substrate into oppositely-charged polycation and polyanion solutions. Adsorption of each individual layer is self-terminated (typically within a few minutes) by completion of the charge reversal. Films can be grown uniformly and homogenously while the thickness can be easily controlled through the number of bilayers (pair of oppositely-charged layers). The technique was originally published by Iler [8], who presented growth of films of oppositely-charged colloidal solutions and the effect of the films thickness to the corresponding interference fringes. This approach was expanded upon by Decher [9] many

---

Abbreviations: MSNP, modified silica nanoparticle; DAR, diazo-resin; ARCs, anti-reflection coatings; RCP, randomly closed packed; ISAMs, ionic self-assembled multilayers

* Corresponding author.
E-mail address: rheflin@vt.edu (J.R. Heflin).

http://dx.doi.org/10.1016/j.jpcs.2015.09.002
0022-3697/© 2015 Elsevier Ltd. All rights reserved.

years later, in which anionic and cationic amphiphile solutions were used to construct a layer-by-layer film. Decher's work laid the foundation for similar films to be created with various other materials including biological compounds [10–13], polyelectrolytes [10–12,14,15], and nanoparticles [13,15,16].

As research on inorganic nanoparticles continues to grow, their applications have spread into catalysis [17–19], biomedical [20–22], electronic [23–25], and optical [26–28], as well as several others. In each of these applications, nanoparticles are useful for their large surface area to volume ratio and dense packing. These properties are also valuable for fabrication of high-quality ARCs. Rubner and colleagues have demonstrated ARCs from layer-by-layer films of SiO_2 nanoparticles and a polycation [29] as well as two different types of nanoparticles [30]. In the former case, they demonstrated mechanical stability of the films through calcination. They have also demonstrated broadband ARCs through multilayer stacks of high and low refractive index layers incorporating TiO_2 and SiO_2 nanoparticles, respectively [31]. Our group [26] has also demonstrated ARCs of ISAM films of poly(allylamine hydrochloride) (PAH) and silica nanoparticles (SiO_2 NPs). The porosity established within the films is directly related to the diameter of the SiO_2 NPs and the corresponding randomly closed packed (RCP) structure. This allows a refractive index near the ideal value for a glass–air interface, determined by the weighted average of that of the SiO_2 NPs and the void space between them. The average refractive index of the film ranged from approximately 1.15–1.45. Three different diameter SiO_2 NPs were examined, and the films constructed with the 45 nm SiO_2 NPs yielded the most effective anti-reflection as their refractive index resided in the range of 1.25–1.35, quite near to the ideal value of 1.22. The films' porosity ranged from 30% to 45%, inversely related to the refractive index of the film. While the porosity is critical to yielding a refractive index for the film near the ideal value, it also significantly weakens the stability of the film both mechanically and in interaction with polar solvents and strongly charged solutions.

The incorporation of the photo-curable crosslinking oligomer, diazo-resin (DAR) 4-diazodiphenylamine/formaldehyde condensate hydrogen sulfate into ionically bonded layer-by-layer films is a promising approach for increasing film stability. DAR is a polycation that allows for the conversion of ionic to covalent bonding with various negatively charged functional groups, by the decomposition of its diazonium group under UV irradiation. Cao et al. [32] placed DAR *in situ* with several polyelectrolyte complex solutions containing sulfonate groups (e.g. PSS, PES) and carboxylic acid groups (e.g. PAA, PSPA, PSPM). They performed crosslinking by photoreaction and thermal methods, which demonstrated resistance to decomposition by ternary solvents. The ternary solvents involved water, DMF, and a salt at a common ratio. Three different salts included in the solvent, LiCl, NaSCN, and $ZnCl_2$, were all shown to be effective at dissolving polyelectrolytes that were not crosslinked. The use of $ZnCl_2$ in the ternary solvent mixture has become a standard means for examining the crosslinking in polyelecytrolyte films. Sun et al. expanded upon the production of covalently stable ISAM films via the polycation of DAR and various polyanions including PSS [33] and PAA [34], as well as porphyrins [35]. Fu et al. [36] and Zhang et al. [37] functionalized nanoparticles to develop ISAM films with DAR as the polycation. In all cases, the films were reported to have increased film stability to solvents after crosslinking.

In this report we demonstrate the encapsulation of SiO_2 NPs with DAR by self-assembly to form a polycation. With a solution of this polycation and a PSS polyanion solution, ISAM films were constructed on glass substrates that were visibly homogenous across the surface. The films displayed peak transmittance values similar to those of Yancey et al. The films exhibit covalent stability in the bulk of the film (crosslinking between DAR and PSS) and on the substrate surface (crosslinking between DAR and grafted sulfonated silanes). The films were characterized by UV–vis spectrometry, scanning electron microscopy (SEM) and atomic force microscopy (AFM) measurements.

2. Experimental

2.1. Materials

4-Diazodiphenylamine/formaldehyde condensate hydrogen sulfate (DAR) (M_w=2,800) was graciously donated by Secant Chemicals. SNOWTEX ST-20L SiO_2 NP solution was purchased from Nissan Chemical, composed of 45 nm average diameter particles, with a concentration of 20 wt%. Poly(styrene sulfonate) (PSS) (M_w=70,000) was purchased from Polysciences Inc. The aqueous solutions were developed and diluted with ultrapure de-ionized water (18 MΩ cm resistivity) (DI water). 95% (3-mercaptopropyl) trimethoxysilane (MPTS) solution was purchased from Sigma-Aldrich. Other reagents used for glass microscope slide preparation were of analytical grade and unaltered for use.

2.2. Instrumentation

The ISAM films were fabricated with a programmable automated immersion system from nanoStrata, Inc. The MSNP films were UV irradiated by a Kinsten KVB-30 exposure unit, which had six 20 W UV fluorescent bulbs. A Zetasizer nanoZS (Malvern Instruments) operating at a fixed angle of 173° and 633 nm wavelength was utilized for ζ-potential and dynamic light scattering (DLS) measurements. The optical transmission, reflection, and absorption spectra were recorded by a Perkin Elmer Lambda 950 UV/VIS and a Filmetrics F10-RT-EXR spectrophotometer. The physical thickness measurements were performed with a Veeco DekTak 150 Stylus Profilometer with a 2.5 μm tip radius stylus and an application of 1 mg force. A LEO 1550 field emission scanning electron microscope (FESEM) unit at an accelerating voltage of 5 kV was used to characterize the morphology.

2.3. Solution formation

The SiO_2 NPs were encapsulated with DAR while in solution, to allow for the SiO_2 NPs to be involved with the crosslinking reaction between DAR and PSS. The encapsulated SiO2 NPs are designated modified silica nanoparticles (MSNPs). In order to identify the conditions under which the SiO_2 NPs are fully covered with DAR without substantial excess remaining in the solution, a range of DAR concentrations were added to the SiO_2 NP solution and mixed for 12 h. The solutions were sonicated for a total of 80 minutes to induce maximum dissolution of potential agglomerates. Schematic representation of the self-assembly directly onto the particles is shown in Fig. 1(a–f).

Through encapsulation, two conditions are satisfied: (1) conversion of the anionic SiO_2 NP solution to cationic (necessary for ionic film growth with a polyanion) (2) the DAR polyelectrolyte chains, on the surface of the MSNPs, could be used for crosslinking with the sulfonate groups of the polyanion PSS after film construction. In this manner, self-assembled encapsulation was carried out in a three-dimensional (3D) architecture in solution, forming nanocomposite shells to later be used in conventional two-dimensional (2D) layer-by-layer film growth. An example of a comparable nanocomposite synthesis was shown by Keller et al. [38], and Pastoriza-Santos et al. [39] produced a similar solution with ZrO_2 nanoparticles encapsulated by DAR. After the encapsulation process, ζ-potential and dynamic light scattering (DLS)

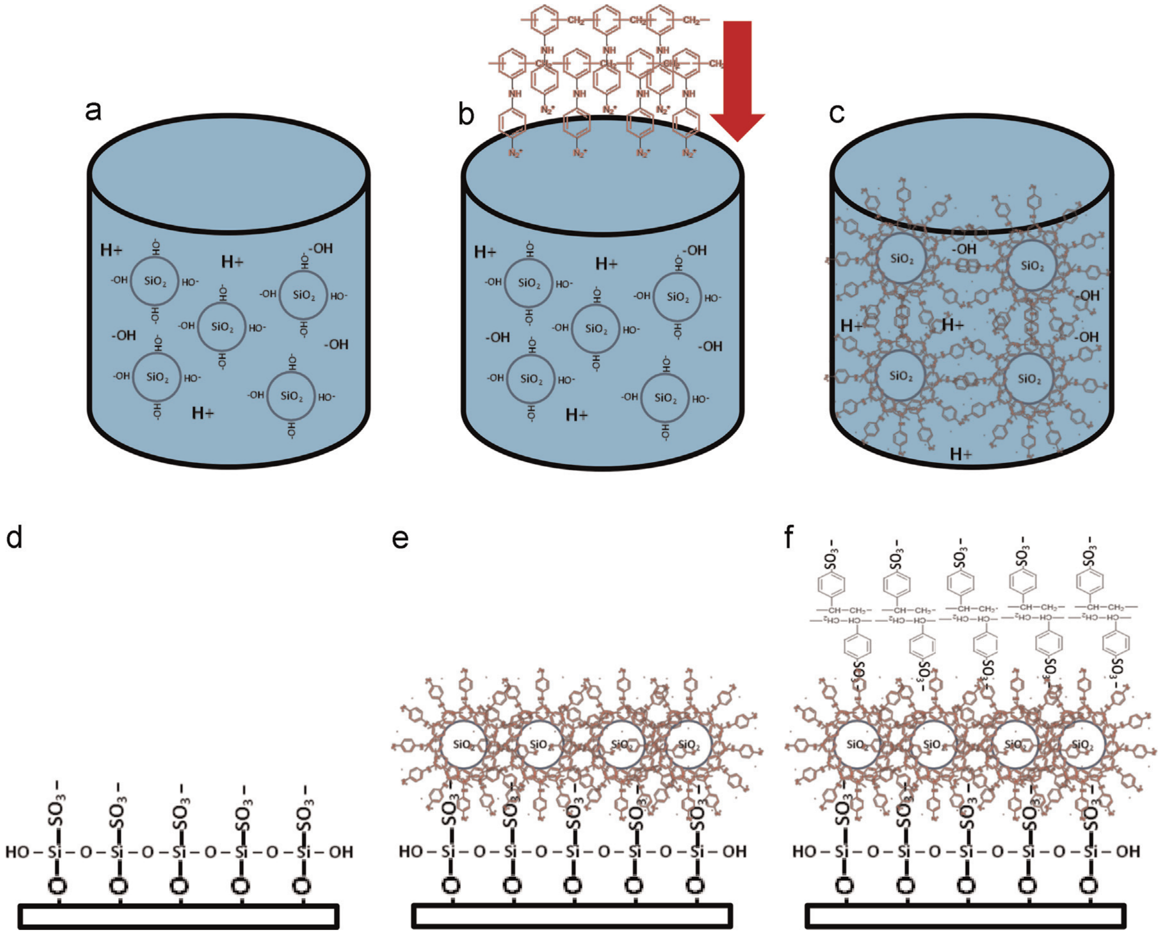

Fig. 1. Schematic of modified silica nanoparticle (MSNP) solution formation: (a) diluted SiO2 NP solution (0.0376 M), (b) deposition of the diazo-resin, (c) encapsulation of the SiO2 NP's by the DAR to make MSNPs. Schematic of ISAM film formation: (d) silylation of glass substrates, (e) growth of the first MSNP polycation monolayer, (f) assembly of the second monolayer, PSS.

measurements by the Zetasizer nanoZS provided characterization of the MSNP surface charge and an indication whether agglomerates were present, respectively.

The PSS solution was created by dissolving 10 mM of PSS powder into DI water at a pH of 7.0.

2.4. Sulfonated silane slide preparation

To provide covalent attachment of the film to the substrate by DAR crosslinking, a procedure nearly identical to that of Wu et al. [40] was carried out to graft silane molecules onto the glass surface and functionalize them with sulfonate groups.

2.5. Film fabrication

The programming parameters of the automated immersion system had a significant effect on the final quality of the ISAM films. The immersion system consists of eight solution positions (one solution at every 45°), with programming that allows for timing of each step. The substrate platform holds four substrates simultaneously (one substrate at every 90°) and can be programmed to spin in the charged solutions at a range of frequencies (600–3000 rpm). After many experimental variations, we settled on an approach that consistently produced films with minimal haze, excellent homogeneity and anti-reflectivity. The substrates were immersed in the MSNP polycation solution for ten minutes per bilayer while spinning in the solution at 3000 rpm. Afterwards, the substrates were rinsed for a total of two minutes and fifteen seconds while spinning at 3000 rpm. The rinsing solutions were refilled for every bilayer with fresh DI water to remove contaminants. The rinsing step eliminated weakly bound particles on the film surface and decreased the overall surface roughness. After rinsing, the substrates were then dipped statically into the polyanion PSS solution for three minutes per bilayer. The substrate platform was kept full (four substrates), during the entire growth to promote uniform current flow as the substrates were spun in the solutions. The fabrication process was maintained in complete darkness to avoid premature decomposition of the DAR in the MSNP solution. Upon termination of ISAM film fabrication, the slides were dried by a stream of N_2 gas and then exposed to UV irradiation for fifteen minutes.

3. Results and discussion

3.1. Modified silica nanoparticle solution formation

Initially, we attempted to deposit polyelectrolytes into an undiluted solution of SiO_2 NPs (3.76 M) in order for encapsulation of the surface on the individual SiO_2 NPs in solution. However, this approach was unsuccessful since individual polyelectrolyte chains were able to coat multiple SiO_2 NPs at once, resulting in large agglomerated particles in the solution (characterized by DLS and SEM). The agglomerates negatively affected the transmission and anti-reflection of the ISAM film through the creation of diffuse light scattering due to the inhomogeneity.

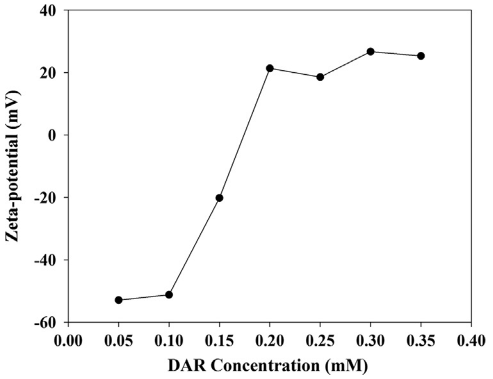

Fig. 2. ζ-potential vs. DAR concentration for the MSNP solution. The solution crosses from negative to positive potential between 0.15 and 0.2 mV. The solution achieved stabilization at 0.25 mV.

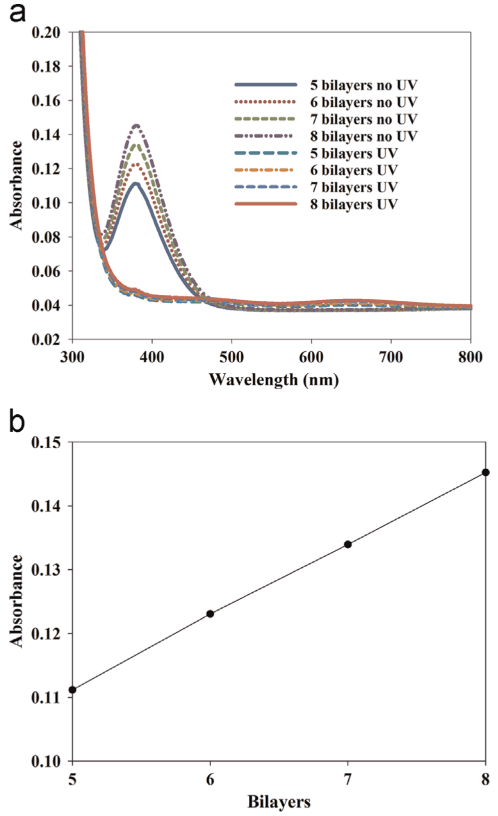

Fig. 3. Absorption spectra for (a) four DAR/PSS films ranging from five to eight bilayers. Spectra are shown before and after UV irradiation exposure. The (b) absorbance vs. bilayers without UV is shown to increase linearly with each bilayer.

A remedy for this situation was dilution of the original SiO_2 NP solution concentration by a factor of to a concentration of 0.0376 M. Dilution of the solution resulted in decreased particle proximity in the colloidal suspension, thus decreasing the probability of particle aggregation. The next step for preparation of the MSNP solution was determination of the most effective concentration for DAR into the diluted SiO_2 NP solution. Five different concentrations of DAR in the range of 0.05–0.35 mM were added to the 0.0376 M SiO_2 NP solution and were mixed for a period of 12 h. Each solution was then sonicated for 80 min to break up any present agglomerates. ζ-Potential and dynamic light scattering (DLS) measurements were performed on each of the solutions by a Zetasizer Nano ZS instrument at 25 °C. By measuring the ζ-potential, we could find the lowest DAR concentration point that resulted in a positively-charged and stable solution, as shown in Fig. 2. A concentration below this point would result in solution instability (precipitation), and a concentration above this point would result in excess DAR in the solution (interfering with the ISAM film growth). The process was performed in the dark to disallow for reactivity of the DAR in the presence of UV irradiation.

A DAR concentration of 0.25 mM into a 0.0376 M SiO_2 NP solution resulted in the best MSNP solutions. Although 0.2 mM was the lowest concentration with a positive surface charge on the NPs, the resultant colloids were unstable. Solution instability was almost instantly apparent, as the solid constituents would visually separate completely or partially from the liquid. At the 0.25 mM concentration, the ζ-potential was 18.6 mV and the average particle size was 115 nm (compared to 64.6 nm for the SiO_2 NP solution prior to the addition of DAR), as measured by DLS. The solution was continuously stirred in a box that restricted light and was sonicated directly before ISAM deposition.

3.2. UV–vis spectrometry

To study the crosslinking and growth behavior of the polyelectrolytes DAR and PSS, films were first constructed without the inclusion of the SiO_2 NPs. Without the SiO_2 NPs, optical interference fringes were not present, allowing clearer observation of the absorption spectra of the polyelectrolytes. Four films ranging from five to eight bilayers were created, solely with the polyelectrolytes and without alteration of their pH conditions. Absorption spectra were taken for the films before and after exposure to UV irradiation. Fig. 3(a,b) shows a linear increase in absorbance with the number of bilayers of DAR/PSS at the wavelength $\lambda = 380$ nm, signifying consistent thickness increments with bilayers.

The location of the absorbance peak at that particular wavelength for the films without UV irradiation is identified as the π–π^* transition of diazonium group [33]. For the spectra of the films that have received the prescribed dosage of UV irradiation, a complete flattening of the characteristic peak at $\lambda = 380$ nm can be observed indicating substantial decomposition of the diazonium groups. Although not entirely conclusive alone, this indicates that crosslinking to create covalent linkages between the DAR and PSS occurred within the films.

Following the evidence of crosslinking of DAR and PSS under UV exposure, this approach was next applied to silica nanoparticle ARCs. As discussed previously, a MSNP solution was formed to combine the porous film architecture of the silica nanoparticles with the crosslinking of the DAR to the polyanionic PSS layer. The ISAM film fabrication conditions were examined to obtain films with the greatest macroscale homogeneity and transmittance levels. Film homogeneity was identified by consistent transmittance and thickness measurements at four different film locations, low roughness value, and by qualitative visual inspection. Importance was placed upon reducing overall roughness values in order to reduce the diffuse light scattering. The film deposition conditions that optimized homogeneity are described in the experimental section. Films were grown in the range of one to four bilayers onto glass substrates treated to provide a sulfonated surface layer. After the films were exposed to UV irradiation to induce the crosslinking reaction between DAR and PSS, transmission and reflection spectra were recorded as shown in Fig. 4(a,b).

The optical thickness (product of refractive index and physical thickness) was calculated for each of the films from the spectra by utilization of the reflection destructive and constructive interference relationships.

$$(m - 0.5)\lambda = 2nd \qquad (1)$$

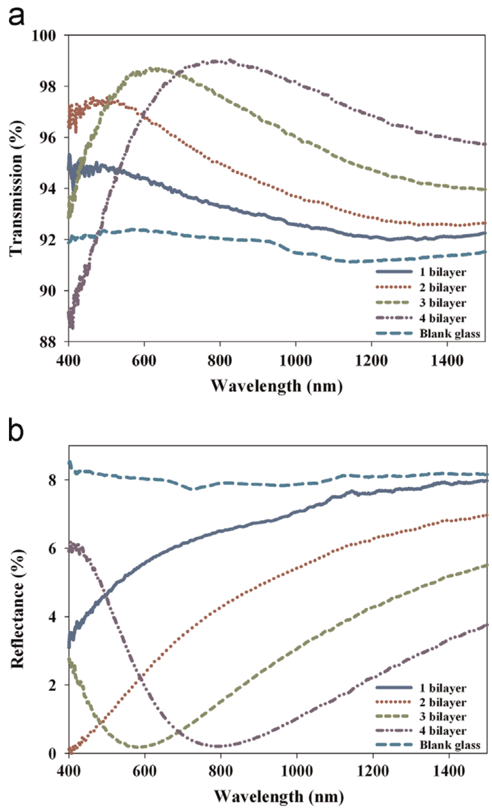

Fig. 4. Transmission (a) and reflection (b) spectra for MSNP/PSS films after UV irradiation exposure. The films range from one to four bilayers.

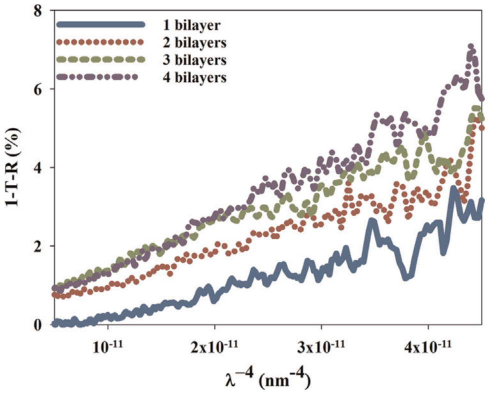

Fig. 5. Extinction vs. λ^{-4} for MSNP/PSS films.

$$m\lambda = 2nd \tag{2}$$

where m is the interference order, λ is the wavelength, n is the refractive index, and d is the physical thickness. Eqs. (1) and (2) are used with the wavelength for transmission maxima and minima for each interference fringe order, respectively. For the reflectance spectra, Eqs. (1) and (2) refer to the minima and maxima, respectively. The transmission maxima and reflectance minima designate the location of the greatest destructive interference for the reflected light for the specific interference fringe order. The optical characteristics of the films are listed in Table 1, where OT is optical thickness, PT is physical thickness, and n is refractive index. The one-bilayer film was excluded from the table, as its primary destructive interference mode for reflection was located outside of the visible wavelength range.

As expected, the wavelength of minimum reflection increases with the number of bilayers, indicating the increased thickness with increased bilayers. From the peak wavelengths, a set of optical thickness values were deduced for the films. The physical thicknesses of the films were found by an average of five step height measurements taken by a profilometer. The refractive index was then obtained from these measurements of the optical and physical thickness. The refractive indices are quite consistent in the range of 1.25–1.26, confirming uniformity of the different bilayers. The values are also close to the ideal anti-reflection refractive index for glass substrates in an environment of air, at 1.22. This supports the high peak transmission levels and low reflection values shown in the table. To better understand the peak transmission values, the extinction for the films was examined. The extinction is defined as 1-T-R and corresponds to absorption and scattering losses. Since the absorption losses from the glass substrate and the film are negligible in the visible range, the observed extinction is therefore assigned almost entirely to light scattering. The scattering intensity versus wavelength, as presented in Fig. 5, was examined to investigate the variation of peak transmission levels between the films.

Given by the slopes for the different films, an overall rise in Rayleigh scattering intensity with an increase of film thickness (bilayers) can be observed from the figure. As light travels through films with larger thicknesses, incident photons interact with a greater number of particles, naturally causing elevated levels of scattering. Rayleigh scattering naturally occurs more strongly at higher wavenumbers (shorter wavelengths), due to the $1/\lambda^4$ dependence. Since Rayleigh scattering is smaller for longer wavelengths, the transmission peaks at longer wavelengths exhibited higher transmittances than those at shorter wavelengths, as seen in Table 1.

3.3. FESEM

To confirm the homogeneity of the MSNP/PSS films on the micro-scale, FESEM was used to qualitatively evaluate the films (for a range of bilayers) and examine possible particle agglomeration. This characterization primarily provided insight for the homogeneity of film growth during stages that the experimental parameters were altered. In the early phases that the MSNP particles were used, poor visible transmittance film levels were obtained and diffuse light scattering could be identified on the films by the lack of transparency (visual cloudiness). By utilization of

Table 1
Optical characteristics for MSNP/PSS films ranging from two to four bilayers.

Bilayers	Transmission max (%)	Reflectance min (%)	Wavelength peak (nm)	Thickness (nm)		Refractive index, *n*	Roughness (nm)
				Optical	Physical		
1	–	–	–	–	62.52	–	5.75
2	97.59	0.015	484	121	95.70	**1.26**	4.20
3	98.73	0.17	620	155	124.0	**1.25**	5.78
4	99.02	0.20	797	199	158.8	**1.25**	5.27

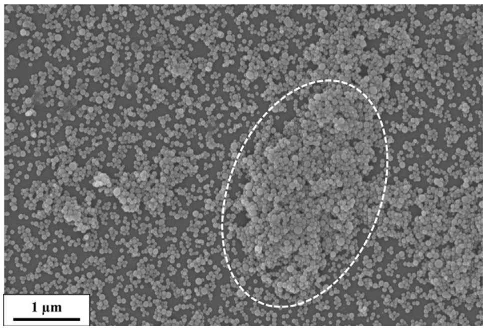

Fig. 6. FESEM characterization of a MSNP/PSS film at 50kX produced from a solution with large agglomerates. A particularly large agglomerate is circled in the figure.

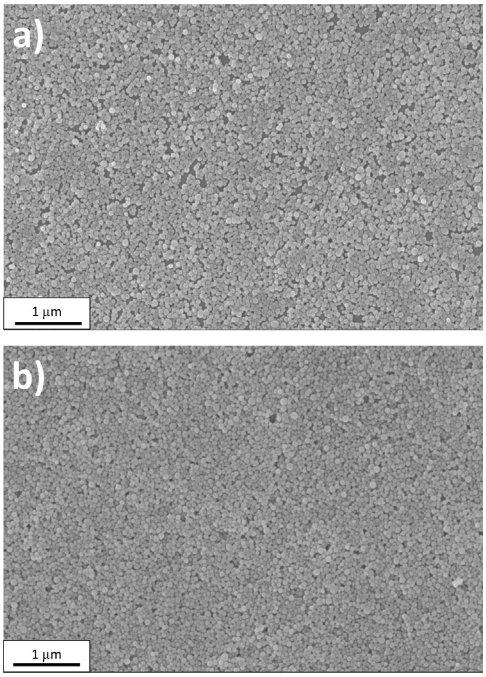

Fig. 7. FESEM characterization of MSNP/PSS films after UV irradiation at 20 kX. Images are shown for (a) a two-bilayer film and (b) an eight-bilayer film.

FESEM characterization, very large (> 1 μm) agglomerations of particles could be distinguished on the surface, shown in Fig. 6.

This necessitated modifications to the MSNP fabrication process to eventually yield a more homogeneous distribution of particles. Fig. 7 represents the final quality of the MSNP fabrication of the ARC ISAM films. For both the two-bilayer and eight-bilayer films, the micrographs show a consistently uniform and homogeneous nano-porous film matrix. The particles are well-distributed on the surface (as confirmed by software measurement tools), which satisfied the required conditions to minimize diffuse light scattering.

3.4. Solvent stability

As previously discussed, the ionic bonding of the polyelectrolytes DAR and PSS exhibits solubility and instability to contact with ternary solvents such as H_2O/N,Ndimethylformamide(DMF)/$ZnCl_2$. Through crosslinking of the polyelectrolytes to form covalent linkages, solvent stability could be achieved [32,33]. After growth of four 10-bilayer MSNP/PSS films, two of the films were left UV unirradiated and two were UV irradiated by the Kinsten KVB-30 exposure unit. The films were then sonicated in a ternary solvent solution of H_2O/DMF/$ZnCl_2$ (3:5:2 w/w/w) for increasing time periods while maintaining an absence of all light. The films were tested for one, two, five, and ten total minutes to develop a relationship of time in the ternary solvent to the degradation of the films determined by absorbance spectra. Since the solvent left a thick residue on the surface of the films, a vigorous rinsing process was performed that involved eight 45-s rinsing steps. This allowed for reproducible and accurate spectral results. Transmission spectra for both sets of films were recorded after each time period and are shown in Fig. 8(a,b).

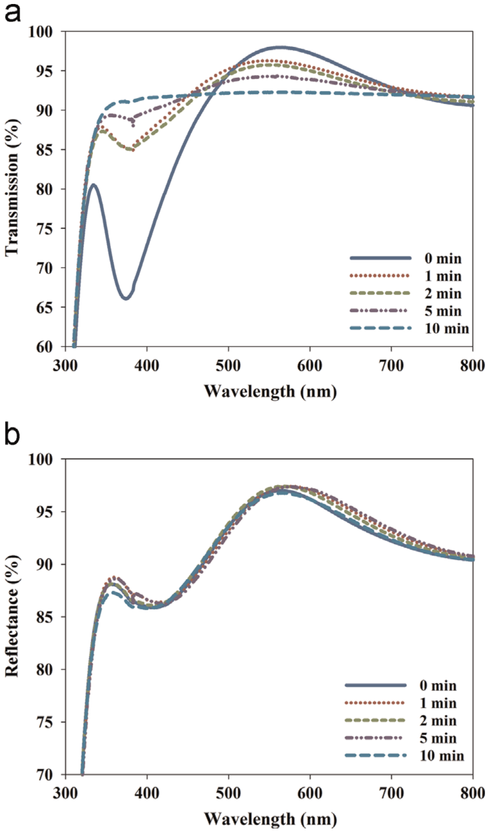

Fig. 8. Transmission spectra for two 10-bilayer MSNP/PSS films after being sonicated in a ternary solvent solution (H_2O/DMF/$ZnCl_2$ (3:5:2)) for various periods of time. (a) One film was UV irradiated and (b) one film was left without UV irradiation.

For the UV irradiated film, the spectra for all of the different exposure times are nearly identical showing that over a period of etching time, the composition of the irradiated film is virtually unchanged. Visual inspection of the film after solvent exposure also showed no observable changes. The film that was not UV irradiated for cross-linking showed different properties. Before etching, a transmission valley at 380 nm defined the strong absorption from the diazonium group as discussed previously. At 566 nm, a transmission peak was formed by the destructive interference of the reflected waves, created by the porous MSNP matrix. After one minute of solvent exposure time, the diazonium absorption decreased (seen as a rise in transmission) and the antireflection peak transmittance dropped considerably. When the film was tested after ten minutes of exposure, the transmission spectrum was similar to that of a bare substrate, which showed that most of the film had been dissolved. Visual inspection of this non-irradiated film, after ten minutes of ternary solvent exposure, showed very little of the original film present.

AFM imaging characterization of the films with and without UV irradiation was conducted to confirm the visual inspection of the film removal on a micro-level. The imaging was completed for both sets of films after their exposure to the ternary solvent for ten

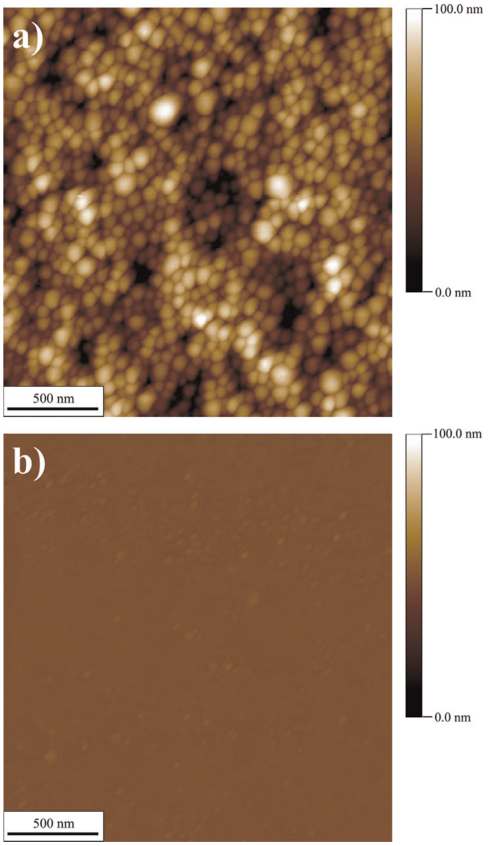

Fig. 9. AFM characterization for two 10-bilayer MSNP films after being sonicated in a ternary solvent solution ($H_2O/DMF/ZnCl_2$ (3:5:2)) for ten minutes. One film was (a) UV irradiated, and the other was (b) not irradiated before immersion in the solvent.

minutes. The height measurement of the film with UV irradiation showed an unaltered MSNP matrix, similar to that shown by the FESEM characterization. For the film without the UV irradiation, the surface was essentially barren of deposited material, as shown in Fig. 9(a,b). This confirmed the instability of the uncrosslinked film to the ternary solvent and the stability of the crosslinked film.

4. Conclusions

Antireflection coating ISAM films were rendered stable against ternary solvents by the introduction of DAR short-chain UV-crosslinkable oligomers. DAR was incorporated by the encapsulation of SiO_2 NPs at a reduced concentration to form a non-agglomerated modified silica nanoparticle solution, referred to as MSNP. With the MSNP polycation solution and the polyanionic PSS solution, highly transparent and homogenous ISAM growth was possible. For visible wavelengths, transmission and anti-reflection levels were optimized at 98.76% and 0.03%, respectively. After UV irradiation, the films showed resilience against ternary solvents that confirmed their stability within the film and to the silylated substrate.

Acknowledgments

This work was done as part of the MultiTASC Materials Center of Excellence at Virginia Tech. Research was sponsored by the Army Research Laboratory and was accomplished under Co-operative Agreement Number W911NF-06-2-0014. The views and conclusions contained in this document are those of the authors and should not be interpreted as representing the official policies, either expressed or implied, of the Army Research Laboratory or the U.S. Government. The U.S. Government is authorized to reproduce and distribute reprints for Government purposes notwithstanding any copyright notation hereon.

The authors gratefully acknowledge the generous donation of DAR oligomers from Secant Chemicals.

References

[1] Y.F. Makableh, R. Vasan, J.C. Sarker, A.I. Nusir, S. Seal, M.O. Manasreh, Sol.r Energy Mater. Sol. Cells 123 (2014) 178–182.
[2] Jorik van de Groep, Pierpaolo Spinelli, Albert Polman, Nano Lett. (2015).
[3] Kang-Soo Han, Ju-Hyeon Shin, Woo-Young Yoon, Heon Lee, Sol. Energy Mater. Sol. Cells 95 (2011) 288–291.
[4] Jing Shi, Zhongrong Geng, Junyan Zhang, Chengbing Wang, Surf. Interface Anal. 46 (2014) 530–534.
[5] Minghua Li, Hui Shen, Lin Zhuang, Daming Chen, Xinghua Liang, Inter. J. Photoenergy 2014 (2014).
[6] Yi-Yu Lee, Wen-Jeng Ho, Chien-Wu Yeh, Appl. Surf. Sci. (2015).
[7] Yen-Tien Lu, Andrew R. Barron, J. Mater. Chem. A 2 (2014) 12043–12052.
[8] R.K. Iler, J. Colloid Interface Sci. 21 (1966) 569–594.
[9] G. Decher, J.D. Hong, Macromol. Symp. 46 (1991) 321–327.
[10] G. Decher, B. Lehr, K. Lowack, Y. Lvov, J. Schmitt, Biosens. Bioelectron. 9 (1994) 677–684.
[11] C. Lu, C. Luo, W. Cao, Colloids Surf., B 25 (2002) 19–27.
[12] N.G. Balabushevitch, G.B. Sukhorukov, N.A. Moroz, D.V. Volodkin, N. I. Larionova, E. Donath, H. Mohwald, Biotechnol. Bioengergy 76 (2001) 207–213.
[13] J.J. Xu, W. Zhao, X.L. Luo, H.Y. Chen, Chem. Commun. 6 (2005) 792–794.
[14] A.A. Antipova, G.B. Sukhorukov, J. Colloid Interface Sci. 111 (2004) 49–61.
[15] T.V. Bukreeva, I.V. Marchenko, B.V. Parakhonskiy, Yu. V. Grigor'ev, Colloid J. 71 (2009) 596–602.
[16] J. Park, L.D. Fouché, P.T. Hammond, Adv. Mater. 17 (2005) 2575–2579.
[17] K. Cho, W.D. Kerber, S.R. Lee, A. Wan, J.D. Batteas, D.P. Goldberg, Inorg. Chem. 49 (2010) 8465–8473.
[18] S. Cheong, J.D. Watt, R.D. Tilley, Nanoscale 2 (2010) 2045–2053.
[19] V. Mazumder, M. Chi, K.L. More, S. Sun, J. Am. Chem. Soc. 132 (2010) 7848–7849.
[20] S. Utech, C. Scherer, M. Maskos, J. Magn. Magn. Mater. 321 (2009) 1386–1388.
[21] B. Bajaj, B.D. Malhotra, S. Choi, Thin Solid Films (2010) 1219–1223.
[22] B.D. Plouffe, D.K. Nagesha, R.S. DiPietro, S. Sridhar, D. Heiman, S.K. Murthy, L. H. Lewis, J. Magn. Magn. Mater. 323 (2011) 2310–2317.
[23] D. Caro, K. Jacob, H. Hahioui, C. Faulmann, L. Valade, T. Kadoya, T. Mori, J. Fraxedasd, L. Viaue, New J. Chem. 35 (2011) 1315–1319.
[24] R. Montazami, S. Liu, Y. Liu, D. Wang, Q. Zhang, J.R. Heflin, J. Appl. Phys. 109 (2011) 104301.
[25] T. Sugino, K. Kiyohara, I. Takeuchi, K. Mukai, K. Asaka, Carbon 49 (2011) 3560–3570.
[26] S.E. Yancey, W. Zhong, J.R. Heflin, A.L. Ritter, J. Appl. Phys. 99 (2006) 034313.
[27] C.Y. Huang, Y.J. Huang, Y.H. Tseng, Opt. Express 17 (2009) 20860–20865.
[28] K.P. Pernstich, M. Schenker, F. Weibel, A. Rossi, W.R. Caseri, ACS Appl. Mater. Interfaces 2 (2010) 639–643.
[29] F.C. Cebeci, Z. Wu, L. Zhai, R.E. Cohen, M.F. Rubner, Langmuir 22 (2006) 2856–2862.
[30] D. Lee, M.F. Rubner, R.E. Cohen, Nano Lett. 6 (2006) 2305–2312.
[31] H. Shimomura, Z. Gemici, R.E. Cohen, M.F. Rubner, ACS Appl. Mater. Interfaces 2 (2010) 813–820.
[32] W.X. Cao, S.J. Ye, S.G. Cao, C. Zhao, Macromol. Rapid Commun. 18 (1997) 983–989.
[33] J. Sun, T. Wu, Y. Sun, Z. Wang, X. Zhang, J. Shena, W. Caob, Chem. Commun. 17 (1998) 1853–1854.
[34] J. Sun, T. Wu, F. Liu, Z. Wang, X. Zhang, J. Shen, Langmuir 16 (2000) 4620–4624.
[35] J. Sun, Z. Wang, Y. Sun, X. Zhang, J. Shen, Chem. Commun. 8 (1999) 693–694.
[36] Y. Fu, H. Xu, S. Bai, D. Qiu, J. Sun, Z. Wang, X. Zhang, Macromol. Rapid Commun. 23 (2002) 256–259.
[37] H. Zhang, R. Wang, G. Zhang, B. Yang, Thin Solid Films 429 (2003) 167–173.
[38] S.W. Keller, S.A. Johnson, E.S. Brigham, E.H. Yonemoto, T.E. Mallouk, J. Am. Chem. Soc. 117 (1995) 12879–12880.
[39] I. Pastoriza-Santos, B. Schöler, F. Caruso, Adv. Funct. Mater. 11 (2001) 122–128.
[40] Chun-Guey Wu, Liang-Feng Tzeng, Yen-Ting Kuo, Chung Hsien Shu, Appl. Catal., A 226 (2002) 199–211.